Hypoxia reduces cell attachment of SARS-CoV-2 spike protein by modulating the expression of ACE2 and heparan sulfate

AUTHORS/AFFILIATIONS

Endika Prieto-Fernández[1], Leire Egia-Mendikute[1], Laura Vila-Vecilla[1], So Young Lee[1], Alexandre Bosch[1], Adrián Barreira-Manrique[1], Ana García-del Río[1], Asier Antoñana-Vildosola[1], Borja Jimenez-Lasheras[1], Asis Palazon[1,2,*]

[1]Cancer Immunology and Immunotherapy Lab, Centre for Cooperative Research in Biosciences CIC bioGUNE, Basque Research and Technology Alliance, Derio, Spain.
[2]Ikerbasque, Basque Foundation for Science, Bilbao, Spain.

*Corresponding author: Asis Palazon (apalazon@cicbiogune.es)

ABSTRACT

A main clinical parameter of Covid-19 pathophysiology is hypoxia. Here we show that hypoxia decreases the attachment of the receptor binding domain (RBD) and the S1 subunit (S1) of the spike protein to epithelial cells. In Vero E6 cells, hypoxia reduces the protein levels of ACE2, which might in part explain the observed reduction of the infection rate. However, hypoxia also inhibits the binding of the spike to human lung epithelial cells lacking ACE2 expression, indicating that hypoxia modulates the expression of additional binding partners of SARS-CoV-2. We show that hypoxia also decreases the total cell surface levels of heparan sulfate, a known attachment receptor of SARS-CoV-2, by reducing the expression of syndecan-1 and syndecan3, the main proteoglycans containing heparan sulfate. Our study indicates that hypoxia acts to prevent SARS-CoV-2 infection, suggesting that the hypoxia signaling pathway might offer therapeutic opportunities for the treatment of Covid-19.

INTRODUCTION

By the end of 2020, SARS-CoV-2 has infected over 54 million people and caused >1.3 million deaths. There is an urgent medical need of developing efficacious and safe vaccines and therapeutic approaches. A common feature of Covid-19 patients is moderate to severe hypoxia (Caputo et al., 2020). Currently, the impact of hypoxia on SARS-CoV-2 infectivity and Covid-19 pathogenesis is unclear, but there are emerging indications that low oxygen concentrations might prevent infection or disease severity (Couzin-Frankel, 2020). This notion is supported by the fact that epidemiological data indicates that Covid-19 severity decreases in high altitude areas (Arias-Reyes et al., 2020). The spike protein of SARS-CoV-2 interacts with both ACE2 and cellular heparan sulfate (HS) through the receptor binding domain (RBD) (Clausen et al., 2020; Walls et al., 2020; Yan et al., 2020). ACE2 expression is regulated by hypoxia on a cell type- and time-dependent manner (Paizis et al., 2005; Zhang et al., 2009). Syndecans, the main cellular HS-containing proteoglycans (HSPGs), are also differentially regulated by hypoxia. For example, the expression of syndecan-1 (sdc-1) in the lungs is reduced under hypoxia (Asplund et al., 2009; Wu et al., 2020). Our hypothesis is that hypoxia influences the cellular attachment of SARS-CoV-2 into host cells by modulating the expression of viral entry and attachment receptors on epithelial cells.

RESULTS

Hypoxia reduces the binding of RBD and S1 to epithelial cells and decreases ACE2 protein levels

In order to understand if hypoxia affects the cellular binding of the SARS-CoV-2 spike protein, we subjected human lung epithelial cells (NCI-H460) or Vero E6 cells to different oxygen concentrations (21% vs. 1% oxygen) and interrogated the binding of RBD and S1. Figure 1A shows a significant decrease of the binding of RBD and S1 after culturing the target cells under hypoxia (1% oxygen) for 24 or 48 hours. To further explore the mechanism responsible for the observed reduced binding of the spike, we assessed *ACE2* gene expression on both cell lines by quantitative PCR (Q-PCR), showing that only Vero E6 cells presented detectable levels of *ACE2* transcripts (Figure 1B). Hypoxia significantly increases *ACE2* transcription on Vero E6 cells (Figure 1C), as expected (Paizis et al., 2005; Shenoy et al., 2020). However, total levels of ACE2 protein decrease after hypoxia exposure (Figure 1D), which might partially explain the reduced cellular binding of RBD. Indeed, Vero E6 cells cultured under hypoxia show a decreased rate of infection with pseudotyped lentiviral particles that were engineered to express the full length spike of SARS-CoV-2 (Figure 1E). However, the spike is also able to bind to NCI-H460, a cell line that contains significantly less abundance of *ACE2* transcripts compared to Vero E6 cells (Figure 1B) and does not express detectable levels of ACE2 protein (Figure 1D). The interaction between the spike and NCI-H460 cells is strongly inhibited by hypoxia (Figure 1A). Altogether, these findings demonstrate the presence of additional SARS-CoV-2 binding factors that are regulated by hypoxia.

Hypoxia decreases the total level of heparan sulfate on the cell surface

We then explored if the levels of cellular HS, a known necessary host attachment factor for SARS-CoV-2, were altered under hypoxia (Figure 2). Hypoxia significantly decreases the total level of cell surface HS on NCI-H460 (Figure 2A) and Vero E6 (Figure 2C) cells. We then assessed the expression of the members of the syndecan family, the main HSPGs on the cell surface, by flow cytometry. Among them, sdc-1 and syndecan-3 (sdc-3) are the most abundant on both cell lines. Hypoxia downregulates the levels of sdc-1 on human lung epithelial cells both at transcriptional (data not shown) and protein levels (Figure 2B), suggesting that sdc-1 is the main contributor to the observed reduction of the total HS pool under hypoxia on NCI-H460

cells. Vero E6 cells also express prominent levels of cell surface sdc-3 that decrease after hypoxia exposure (Figure 2D).

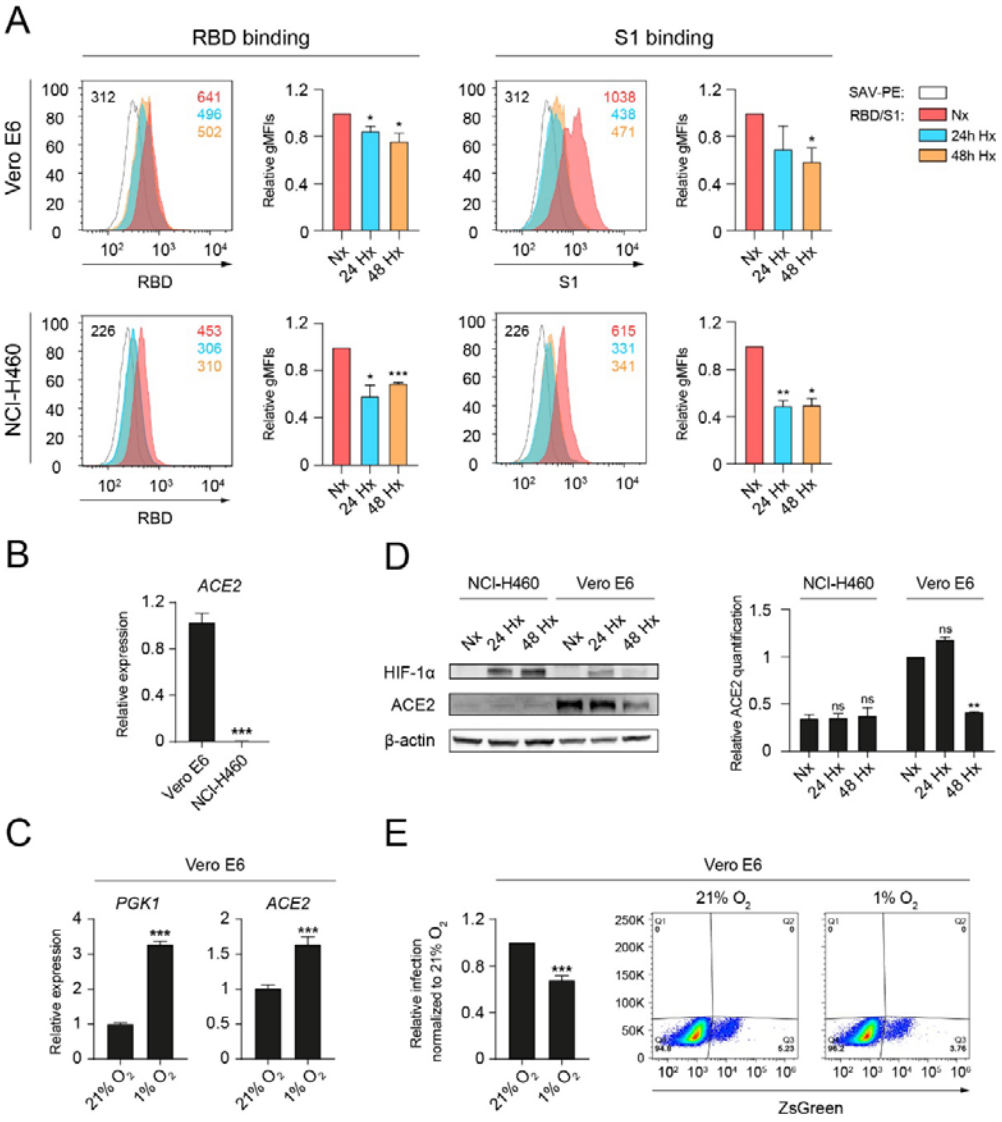

Figure 1. ***Hypoxia reduces the binding of RBD and S1 to epithelial cells and decreases ACE2 protein levels***. (***A***) Binding of the receptor binding domain (RBD) (*left*) or S1 subunit (S1) (*right*) to Vero E6 (*top*, n=3, unpaired t test) or NCI-H460 (*bottom*, n=2, unpaired t test) cells cultured under normoxia (21% oxygen) or hypoxia (1% oxygen) for 24 and 48 hours, measured by flow cytometry. A representative histogram indicating the geometric mean fluorescent intensity (gMFI) value for each condition is shown. (***B***) Relative *ACE2* gene expression on Vero E6 and NCI-H460 measured by Q-PCR (n=3, unpaired t test). (***C***) Relative gene expression of *PGK1* (*left*) and *ACE2* (*right*) on Vero E6 cells cultured under normoxia or hypoxia for 24 hours (n=3, unpaired t test). (***D***) (*Left*) Western blot of HIF-1α, ACE2 and β-actin on Vero E6 and NCI-H460 cells cultured under normoxia or hypoxia for the indicated time points. (*Right*) Relative quantification of ACE2 protein expression by densitometry (n=2, 2-way ANOVA). (**E**) Relative infection of Vero E6 cells with pseudotyped viral particles expressing the spike protein of SARS-CoV-2, measured by flow cytometry based on ZsGreen expression (n=4 independent experiments). Error bars represent SEM. Asterisks represent p values (*, ≤ 0.05; **, < 0.01; ***, < 0.001).

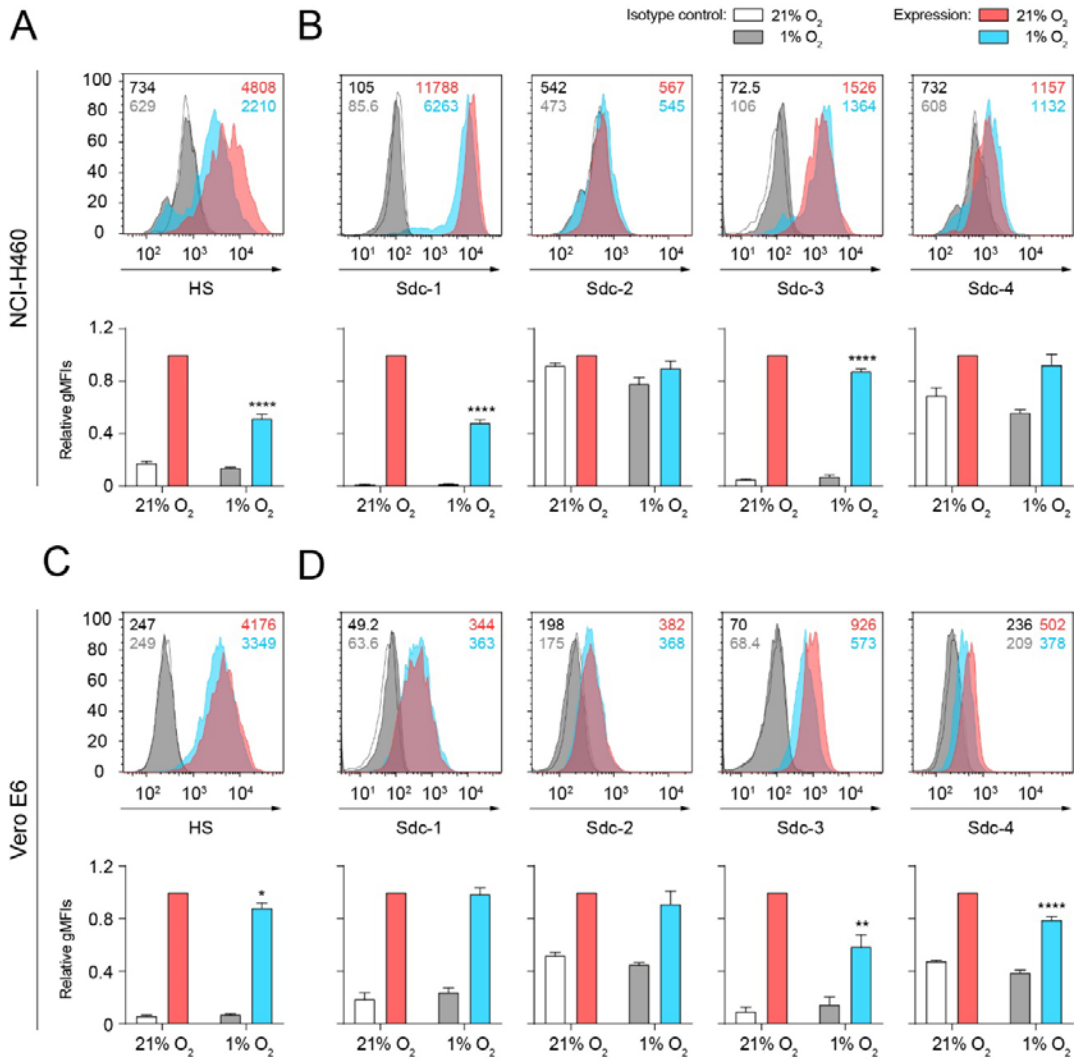

Figure 2. ***Hypoxia decreases the total level of heparan sulfate on the cell surface***. (***A, B***) Total heparan sulfate levels (***A***) and expression of Sdc-1 to Sdc-4 (***B***) on NCI-H460 cells cultured under normoxia (21% oxygen) or hypoxia (1% oxygen) for 24 hours, measured by flow cytometry. *(Top)* Histograms show representative results, numerical gMFI values are depicted. (*Bottom*) Bar graphs represent relative gMFI values of a pool of two independent experiments (2-way ANOVA). (***C, D***) The same experiments shown in (***A***) and (***B***) performed in Vero E6 cells. Error bars represent SEM, and asterisks represent p values (*, ≤ 0.05; **, < 0.01; ****, ≤ 0.0001).

DISCUSSION

Covid-19 disease is associated with hypoxia (Caputo et al., 2020), which results on decreased oxygen availability for tissues. This phenomenon affects the susceptibility of host cells to viral infections (Gan and Ooi, 2020) and shapes immune responses (Palazon et al., 2014). Here we describe the binding ability of the spike of SARS-CoV-2 to epithelial cells under different oxygen concentrations.

We show that ACE2, the main SARS-CoV-2 entry receptor, is downregulated under hypoxia. Moreover, hypoxia reduced the infection rate of Vero E6 cells by pseudotyped SARS-CoV-2 lentiviral particles. The observed reduction of ACE2 protein level contrasts with the early transcriptional increase of this gene, a well-documented observation that likely results from the binding of the hypoxia inducible factor (HIF) transcription factors to hypoxia response elements on the *ACE2* promoter (Liu et al., 2020). The observed discrepancy at the RNA *vs.* protein ACE2 levels might be explained by protein degradation, cleavage (Heurich et al., 2014) or time-dependent adaptation to hypoxia. Apart from ACE2, other cell surface proteins contribute to the initial attachment of the virus to the host cells through the interaction of the RBD with HS polysaccharides (Clausen et al., 2020) that decorate HSPGs on the cell surface. Hypoxia decreases the total cell level of HS that is available for the binding of the spike. This reduction might be explained by the hypoxic downregulation of sdc-1 or sdc-3, the most abundant HSPGs present on the cell models tested herein.

In summary, we show that hypoxia decreases the binding of the spike to epithelial cells by at least two different mechanisms: 1) decreasing the level of ACE2 (entry receptor); and 2) reducing the level of HS within the HSPGs (attachment factors) on the cell surface. The significance of these findings at physiopathological oxygen levels remains unexplored. In this context, elucidating the role of the HIF signalling pathway might unlock novel therapeutic targets that, when modulated, reduce the initial virus-host interaction and viral load.

MATERIALS AND METHODS

Key Resources Table

Reagent type (species) or resource	Designation	Source or reference	Identifiers	Additional information
Antibody	ACE2	Bioss antibodies	Cat#: bsm-52614R	1:200 dilution
Antibody	Anti-HS	Amsbio	Cat#: 370255-S	1:200 dilution. Clone F58-10E4.
Antibody	Anti-IgM-FITC	Miltenyi Biotec	RRID:AB_10829949	1:500 dilution
Antibody	Anti-Mo-HRP	Cell Signaling	Cat#: S301677076S	1:5000 dilution
Antibody	Anti-Rb-HRP	Cell Signaling	Cat#: S301677074S	1:5000 dilution
Antibody	HIF-1α	Novus	Cat#: NB100-449	1:100 dilution
Antibody	Syndecan-1	BD	Cat#: 565943	1:100 dilution
Antibody	Syndecan-2	R&D	Cat#: FAB2965P	1:100 dilution
Antibody	Syndecan-3	R&D	Cat#: FAB3539A	1:100 dilution
Antibody	Syndecan-4	R&D	Cat#: FAB291819	1:100 dilution
Cell culture medium	DMEM	Gibco	Cat#: 41966-029	10% FBS and 1% PS antibiotic

Cell culture medium	MEM	Gibco	Cat#: 31095-029	10% FBS and 1% PS antibiotic
Cell culture medium	RPMI	Gibco	Cat#: 61870044	10% FBS and 1% PS antibiotic
Cell line	HEK 293T	Takara	Cat#: 632180	
Cell line	NCI-H460	DSMZ	RRID:CVCL_0459	
Cell line	Vero E6	ATCC	RRID:CVCL_0574	
Chemical compound, drug	7-AAD	BD	RRID:AB_2869266	
Chemical compound, drug	BSA	Sigma	Cat#: A9647	
Chemical compound, drug	Cell dissociation buffer	Thermo	Cat#: 13151-014	
Chemical compound, drug	LDS sample buffer	Invitrogen	Cat#: NP0007	
Chemical compound, drug	M-MLV reverse transcriptase	Thermo	Cat#: 28025-013	
Chemical compound, drug	PageRuler	Thermo	Cat#: 26619	
Chemical compound, drug	PBS	Fisher	Cat#: BP3994	
Chemical compound, drug	Random primers	Thermo	Cat#: 58875	
Chemical compound, drug	Skin milk	Millipore	Cat#: 70166	5%
Chemical compound, drug	Streptavidin PE	Thermo	Cat#: 12-4317-87	1:200 dilution
Chemical compound, drug	SYBR Green	Quantabio	Cat#: 95056-500	
Chemical compound, drug	Tween-20	Sigma	Cat#: 9005-64-5	0,5%
Commercial assay or kit	0.45 µm filter	VWR	Cat#: 514-0063	
Commercial assay or kit	7.5% Mini-PROTEAN TGX gels	BioRad	Cat#: 4561023	
Commercial assay or kit	96-well plates	Thermo	Cat#: 249570	
Commercial assay or kit	BCA Protein Assay kit	Thermo	Cat#: 23227	
Commercial assay or kit	Clarity Max ECL substrate	BioRad	Cat#: 170506	
Commercial assay or kit	jetPEI kit	Polyplus-transfection	Cat#: 101-10N	
Commercial assay or kit	Lenti-X Concentrator	Takara	Cat#: 631231	
Commercial assay or kit	NucleoSpin RNA kit	Macherey-Nagel	Cat#: 740955.250	
Commercial assay or kit	PVDF membrane	BioRad	Cat#: 1704156	
Peptide, recombinant protein	Biotinylated RBD	Acrobiosystems	Cat#: SPD-C82E9	20 µg/mL
Peptide, recombinant protein	Biotinylated S1	Acrobiosystems	Cat#: S1N-C82E8	20 µg/mL

Plasmid	HDM-Hgpm2	Bei resources	Cat#: NR-52517	1.27 µg
Plasmid	HDM-tat1b	Bei resources	Cat#: NR-52518	1.27 µg
Plasmid	Lentiviral backbone (ZsGreen)	Bei resources	Cat#: NR-52520	5.79 µg
Plasmid	pRC-CMV-Rev1b	Bei resources	Cat#: NR-52519	1.27 µg
Plasmid	SARS-CoV-2 spike protein	Bei resources	Cat#: NR-52514	1.97 µg
Software	FlowJo	BD	RRID:SCR_008520	Version 10
Software	ImageJ	ImageJ	RRID:SCR_003070	
Software	QuantStudio	Thermo	RRID:SCR_018712	Version 1.3

Cell Culture. The NCI-H460 cell line was obtained from the DSMZ (German Collection of Microorganisms and Cell Lines Cat#: ACC737) and cultured in RPMI medium 1640 GlutaMAX (Gibco Cat#: 61870044) according to standard culture protocols. Vero E6 cells (ATCC Cat#: CRL-1586) were kindly provided by Nicola G.A. Abrescia (CIC bioGUNE) and cultured in MEM (Gibco Cat#: 31095-029). HEK 293T cells (Takara Bio Inc. Cat#: 632180) were cultured in DMEM (Gibco Cat#: 41966-029). Medium was supplemented with 10% FBS and 1% Penicillin-Streptomycin. Hypoxia cultures were performed at 1% oxygen and 5% CO_2 in an In Vivo2 400 hypoxic station (Ruskinn Technologies).

Binding of RBD and S1 to the cell surface. After culture, cells were collected with cell dissociation buffer (Thermo Fisher Cat#: 13151-014), distributed in 96-well polystyrene conical bottom plates (Thermo Fisher Cat#: 249570) and washed with PBS (Fisher BioReagents Cat#: BP3994) containing 0.5% BSA (Sigma Aldrich Cat#: A9647) (blocking buffer). Cells were incubated with biotinylated S1 (Acrobiosystems Cat#: S1N-C82E8) or RBD (Acrobiosystems Cat#: SPD-C82E9) proteins (20 µg/mL) in blocking buffer for 30 minutes at 4°C. After incubation, cells were washed with 200 µL of blocking buffer and incubated with streptavidin-PE (Thermo Fisher Cat#: 12-4317-87) diluted in 100 µL of blocking buffer (1:200 dilution). All centrifugation steps were performed at 300 x *g* for 5 min (4°C).

Generation of pseudotyped lentiviral particles. Pseudotyped lentiviral particles were generated by transfecting HEK 293T cells as described in (Crawford et al., 2020), using a five plasmid system kindly provided by June Ereño (CIC bioGUNE). Confluent HEK 293T cells (50-70%) were transfected with plasmids encoding for the lentiviral backbone (containing a CMV promoter to express ZsGreen) (NR-52520, 5.79 µg), the SARS-CoV-2 spike protein (NR-52514, 1.97 µg), HDM-Hgpm2 (NR-52517, 1.27 µg), pRC-CMV-Rev1b (NR-52519, 1.27 µg) and HDM-tat1b (NR-52518, 1.27 µg), using the jetPEI kit (Polyplus-transfection Cat#: 101-10N). 48 hours after transfection, the viruses were harvested from the supernatant, filtered through a 0.45 µm filter (VWR Cat#: 514-0063), concentrated using Lenti-X Concentrator (Takara Bio Inc. Cat#: 631231) and stored in PBS at -80ºC until use.

Titration of the pseudotyped lentiviral particles and infection of Vero E6 cells. Viral titration was performed in Vero E6 cells as described in (Crawford et al., 2020). For single-infection experiments, 150.000 cells were seeded in 6-well plates, left attaching to the bottom overnight in normoxia (21% O2) and incubated for additional 24 hours under normoxia or hypoxia (1% O2). After that, cells were incubated with the pseudotyped lentiviral particles (MOI= 0.1) for 48 hours under normoxic conditions. The infected cells expressed ZsGreen, allowing the detection by flow cytometry.

Flow cytometry. Cells were collected, washed with blocking buffer and incubated with fluorochrome-conjugated antibodies (1:100 dilution in blocking buffer) against syndecan-1 (BD Biosciences Cat#: 565943), syndecan-2 (R&D Systems Cat#: FAB2965P), syndecan-3 (R&D Systems Cat#: FAB3539A) and syndecan-4 (R&D Systems Cat#: FAB291819) for 15 minutes at 4°C. Total heparan sulfate (HS) was measured by flow cytometry after incubation for 30 minutes at 4°C with an anti-HS primary antibody (Amsbio Cat#: 370255-S; clone F58-10E4) (1:200 dilution in blocking buffer). After that, cells were washed and incubated with an anti-IgM FITC-conjugated secondary antibody (Miltenyi Biotec Cat#: 130-095-906) (1:500 dilution in blocking buffer). 7-AAD (BD Biosciences Cat#: 51-68981E) was used to discriminate alive cells. Finally, cells were washed twice, resuspended in 200 µL of blocking buffer and acquired on a FACSymphony cytometer (BD Biosciences). The results were analyzed using FlowJo version 10 (BD Biosciences).

Q-PCR. Total RNA was isolated using the NucleoSpin RNA kit (Macherey-Nagel Cat#: 740955.250). The cDNA was synthesized by RT-PCR from 1 µG of purified RNA with the M-MLV reverse transcriptase (Thermo Fisher Cat#: 28025-013) and random primers (Thermo Fisher Cat#: 58875). The Q-PCR reactions were conducted in triplicate on a ViiA 7 Real-Time PCR system (Thermo Fisher) from 1 µL of cDNA using the PerfeCTa SYBR Green SuperMix reagent (Quantabio Cat#: 95056-500) and gene-specific primers. The amplification program consisted of initial denaturation at 95°C for 3 min followed by 40 cycles of denaturation at 95°C for 15 s, annealing at 60°C for 60 s and extension at 72°C for 60 s. Data were analyzed using the QuantStudio software version 1.3 (Thermo Fisher). The relative quantification in gene expression was determined using the $2^{-\Delta\Delta Ct}$ method by using the *RPLP0* gene as a house-keeping gene (Fw: 5'-CGACCTGGAAGTCCAACTAC-3' and Rv: 5'-ATCTGCTGCATCTGCTTG-3'). *PGK1*, a well-stablished target gene of HIF-1α, *was* used as a control for the hypoxia condition (Fw: 5'- CCGCTTTCATGTGGAGGAAGAAG-3' and Rv: 5'-CTCTGTGAGCAGTGCCAAAAGC-3'). The primer sequences for *ACE2* and *SDC1* expression on human NCI-H460 cells were previously described by (Ma et al., 2020) and (Reynolds et al., 2016), respectively. As these oligos presented several mismatches with the reference sequence of the African green monkey (Vero E6 cells), we designed the following primers to amplify the *ACE2* (Fw: 5'-AGCACTCACGATTGTTGGGA-3' and Rv: 5'- CCACCCCAACTATCTCTCGC-3') and *SDC1* (Fw: 5'-GGGGCTCATCTTTGCTGTGT-3' and Rv: 5'-AAGGAGTAGCTGCCTTCGTC-3') genes.

Western Blot. Total cell lysates were collected using RIPA buffer and quantified with the BCA Protein Assay kit (Thermo Fisher Cat#: 23227). Samples were mixed with LDS sample buffer (Invitrogen Cat#: NP0007) containing DTT, boiled for 15 minutes, separated in a 7.5% Mini-PROTEAN TGX precast protein gel (BioRad Cat#: 4561023) and transferred to a 0.2 µm PVDF membrane (BioRad Cat#: 1704156) using a Trans-Blot Turbo transfer system (BioRad). PageRuler protein ladder (Thermo Fisher Cat#: 26619) was used to estimate the molecular weight of the proteins. The membranes were blocked for 1 hour in 5% skim milk (Millipore Cat#: 70166) and 0.5% Tween-20 (Sigma Aldrich Cat#: 9005-64-5) diluted in PBS. The membranes were probed overnight at 4°C with primary antibodies diluted in PBS containing 5% BSA and 0.5% Tween-20, washed five times with PBS (containing 0.5% Tween-20), incubated for 1 hour at RT with the corresponding secondary HRP-conjugated antibodies (1:5000 diluted in 5% skim milk and 0.5% Tween-20 diluted in PBS) and washed for five additional times. The membranes were probed with antibodies against HIF-1α (Novus Biologicals Cat#: NB100-449), ACE2 (Bioss antibodies Cat#: bsm-52614R) and β-actin (Cell Signaling Cat#: D6A8). The HRP-conjugated secondary antibodies against mouse (Cat#: S301677076S) and rabbit (Cat#: S301677074S) were obtained from Cell Signaling. Chemiluminescence detection was performed using Clarity Max Western ECL Substrate (BioRad Cat#: 170506) on an iBright system (Invitrogen). Band densitometry was performed using ImageJ (https://imagej.nih.gov/ij/).

ACKNOWLEDGEMENTS

A.P. received funding from the European Research Council (ERC), grant agreement number 804236 (Horizon 2020) and the FERO Foundation.

COMPETING INTERESTS

The authors declare no competing interest.

REFERENCES

Arias-Reyes, C., Zubieta-DeUrioste, N., Poma-Machicao, L., Aliaga-Raduan, F., Carvajal-Rodriguez, F., Dutschmann, M., Schneider-Gasser, E.M., Zubieta-Calleja, G., and Soliz, J. (2020). Does the pathogenesis of SARS-CoV-2 virus decrease at high-altitude? Respir Physiol Neurobiol *277*, 103443.

Asplund, A., Ostergren-Lunden, G., Camejo, G., Stillemark-Billton, P., and Bondjers, G. (2009). Hypoxia increases macrophage motility, possibly by decreasing the heparan sulfate proteoglycan biosynthesis. J Leukoc Biol *86*, 381-388.

Caputo, N.D., Strayer, R.J., and Levitan, R. (2020). Early Self-Proning in Awake, Non-intubated Patients in the Emergency Department: A Single ED's Experience During the COVID-19 Pandemic. Acad Emerg Med *27*, 375-378.

Clausen, T.M., Sandoval, D.R., Spliid, C.B., Pihl, J., Perrett, H.R., Painter, C.D., Narayanan, A., Majowicz, S.A., Kwong, E.M., McVicar, R.N.*, et al.* (2020). SARS-CoV-2 Infection Depends on Cellular Heparan Sulfate and ACE2. Cell *183*, 1043-1057 e1015.

Couzin-Frankel, J. (2020). The mystery of the pandemic's 'happy hypoxia'. Science *368*, 455-456.

Crawford, K.H.D., Eguia, R., Dingens, A.S., Loes, A.N., Malone, K.D., Wolf, C.R., Chu, H.Y., Tortorici, M.A., Veesler, D., Murphy, M.*, et al.* (2020). Protocol and Reagents for Pseudotyping Lentiviral Particles with SARS-CoV-2 Spike Protein for Neutralization Assays. Viruses *12*.

Gan, E.S., and Ooi, E.E. (2020). Oxygen: viral friend or foe? Virol J *17*, 115.

Heurich, A., Hofmann-Winkler, H., Gierer, S., Liepold, T., Jahn, O., and Pohlmann, S. (2014). TMPRSS2 and ADAM17 cleave ACE2 differentially and only proteolysis by TMPRSS2 augments entry driven by the severe acute respiratory syndrome coronavirus spike protein. J Virol *88*, 1293-1307.

Liu, A., Zhang, X., Li, R., Zheng, M., Yang, S., Dai, L., Wu, A., Hu, C., Huang, Y., Xie, M., and Chen, Q. (2020). Overexpression of the SARS-CoV-2 receptor ACE2 is induced by cigarette smoke in bronchial and alveolar epithelia. J Pathol.

Ma, D., Chen, C.B., Jhanji, V., Xu, C., Yuan, X.L., Liang, J.J., Huang, Y., Cen, L.P., and Ng, T.K. (2020). Expression of SARS-CoV-2 receptor ACE2 and TMPRSS2 in human primary conjunctival and pterygium cell lines and in mouse cornea. Eye (Lond) *34*, 1212-1219.

Paizis, G., Tikellis, C., Cooper, M.E., Schembri, J.M., Lew, R.A., Smith, A.I., Shaw, T., Warner, F.J., Zuilli, A., Burrell, L.M., and Angus, P.W. (2005). Chronic liver injury in rats and humans upregulates the novel enzyme angiotensin converting enzyme 2. Gut *54*, 1790-1796.

Palazon, A., Goldrath, A.W., Nizet, V., and Johnson, R.S. (2014). HIF transcription factors, inflammation, and immunity. Immunity *41*, 518-528.

Reynolds, M.R., Singh, I., Azad, T.D., Holmes, B.B., Verghese, P.B., Dietrich, H.H., Diamond, M., Bu, G., Han, B.H., and Zipfel, G.J. (2016). Heparan sulfate proteoglycans mediate Abeta-induced oxidative stress and hypercontractility in cultured vascular smooth muscle cells. Mol Neurodegener *11*, 9.

Shenoy, N., Luchtel, R., and Gulani, P. (2020). Considerations for target oxygen saturation in COVID-19 patients: are we under-shooting? BMC Med *18*, 260.

Walls, A.C., Park, Y.J., Tortorici, M.A., Wall, A., McGuire, A.T., and Veesler, D. (2020). Structure, Function, and Antigenicity of the SARS-CoV-2 Spike Glycoprotein. Cell *181*, 281-292 e286.

Wu, F., Wang, J.Y., Chao, W., Sims, C., and Kozar, R.A. (2020). miR-19b targets pulmonary endothelial syndecan-1 following hemorrhagic shock. Sci Rep *10*, 15811.

Yan, R., Zhang, Y., Li, Y., Xia, L., Guo, Y., and Zhou, Q. (2020). Structural basis for the recognition of SARS-CoV-2 by full-length human ACE2. Science *367*, 1444-1448.

295 Zhang, R., Wu, Y., Zhao, M., Liu, C., Zhou, L., Shen, S., Liao, S., Yang, K., Li, Q., and Wan, H.
296 (2009). Role of HIF-1alpha in the regulation ACE and ACE2 expression in hypoxic human
297 pulmonary artery smooth muscle cells. Am J Physiol Lung Cell Mol Physiol *297*, L631-640.